Philosophical Magazine

ISSN: (Print) (Online) Journal homepage: https://www.tandfonline.com/loi/tphm20

Effect of octahedral cation on electronic, magnetic and optic properties of CoX_2O_4 ($X = Cr$, Mn and Fe) spinel compound

N. Hetache, Z. Charifi, T. Ghellab, H. Baaziz & F. Soyalp

To cite this article: N. Hetache, Z. Charifi, T. Ghellab, H. Baaziz & F. Soyalp (2021): Effect of octahedral cation on electronic, magnetic and optic properties of CoX_2O_4 ($X = Cr$, Mn and Fe) spinel compound, Philosophical Magazine, DOI: 10.1080/14786435.2021.1987546

To link to this article: https://doi.org/10.1080/14786435.2021.1987546

Published online: 09 Oct 2021.

PHILOSOPHICAL MAGAZINE
https://doi.org/10.1080/14786435.2021.1987546

Taylor & Francis
Taylor & Francis Group

Effect of octahedral cation on electronic, magnetic and optic properties of CoX_2O_4 ($X = Cr$, Mn and Fe) spinel compound

N. Hetache[a,b], Z. Charifi[a,b], T. Ghellab[a,b], H. Baaziz[a,b] and F. Soyalp[c]

[a]Department of Physics, Faculty of Science, University of M'sila, M'sila, Algeria; [b]Laboratory of Physics and Chemistry of Materials, University of M'sila, M'sila, Algeria; [c]Theoretical Physics Research Laboratory, Department of Mathematics and Science, Faculty of Education, Yüzüncü Yıl University, Tuşba Van, Turkey

ABSTRACT

The magnetic, structural and optical properties of CoX_2O_4 ($X = Cr$, Mn and Fe) spinels are calculated using GGA + U approximation. The effect of the octahedral cation X on the properties of these spinels are analyzed. In order to better understand the electronic aspect of these compounds we studied the issue between the relative forces of the exchange effect and the crystal field effect through a complete analysis of the densities of electronic states. Obtaining the correct ground state is only possible if the electron–electron interactions between magnetic cations are introduced. When the X cations are changed, the crystalline structure changes totally from cubic normal spinel for $CoFe_2O_4$ to tetragonal normal spinel one for $CoMn_2O_4$ to inverse spinel for $CoCr_2O_4$. The electronic properties of our spinels are significantly different, an increase in the band gap from Fe to Mn to Cr compounds is obtained. Magnetic exchange interactions are strongly affected by sub-lattices occupation in the inverse phase of $CoFe_2O_4$ and significant structural distortion of the $CoMn_2O_4$ compound. The analysis of structural parameters and electronic structures plays a role on the trends of magnetic exchange interactions. We have noticed that the iron states in $CoFe_2O_4$ are extremely localised making this spinel very different from the X cation states in the other two spinels. So the variation in X cations allows us to confirm the trend in the properties of CoX_2O_4. The prediction of optical properties is possible and it allowed us to calculate different optical parameters. We have noticed that $\varepsilon_1(0)$ decreases with increasing band gap.

ARTICLE HISTORY
Received 2 July 2021
Accepted 23 September 2021

KEYWORDS
Spinel; hubbard; cobalites; magnetic moment; structural; optical properties

CONTACT Z. Charifi charifizoulikha@gmail.com Department of Physics, Faculty of Science, University of M'sila, M'sila 28000, Algeria

1. Introduction

In recent years, there has been a renewed interest in materials that are strongly coupled in the degrees of freedom of charge and rotation. Systems with an interaction between electronic and magnetic properties, ranging from colossal magneto-resistive materials [1] to dilute magnetic semiconductors [2], have contributed to the determination of the behaviour of these materials and have led to a deeper appreciation of the role of spin-charge coupling.

For many decades, semiconductor oxides having a spinel structure have attracted considerable attention because, in addition to belonging to the class of technologically important materials [3–7], they provide an understanding of coupling, magnetic interactions and electron–electron correlations. The challenges of magnetic spinels are largely due to the understanding of the complexities arising from the different magnetic interactions between different magnetic cations at unequal crystallographic sites.

A member of the spinel oxide family, $CoCr_2O_4$ has attracted considerable attention because of the reversal of magnetisation of ferroelectric polarisation in this oxide. Subsequent studies, aimed at exploring the multiferroic nature of this material, have highlighted the magneto-caloric properties dependent on the illumination temperature and the magnetic field. The magnetic phase diagram of this spinel is rich. A transformation into a collinear ferromagnetic order at 93 K to a complex conical spin spiral of immeasurable complexity at about 26 K [8, 9]. $CoCr_2O_4$ has a normal spinel structure with Co^{2+} ions occupying the tetrahedrally symmetric *A* sites and Cr^{3+} ions occupying the octahedrally symmetric *X* sites and the conical order of the Cr^{3+} sub-lattice is responsible for the magneto-electric coupling in this spinel [10]. This is in agreement with the LKDM (Lyons, Kaplan, Dwight, and Menyuk) theory [11], which using a simple Heisenberg model, shows that the magnetic order in the cubic spinel oxides is determined from the magnetic exchange interactions between *A*-*X* and *X*-*X* ions. However, at low temperature, experimental as well as theoretical work has shown that the magnetic exchange interactions of the *A* sites cannot be neglected [12–14]. Then the electrical polarisation and the magnetic order are influenced by significant changes in magnetic interactions that are directly related to the variations in the occupations of the *A* and *X* sub-lattices.

The high magnetostriction [15] and a critical temperature lead to new magnetic phenomena such as the reversal of the sign of the exchange bias effect [16–18] and the magnetic compensation by substituting chromium atoms with iron. In addition, the substitution of chromium atoms by manganese atoms in $CoCr_2O_4$ leads to a compensation of the magnetisation induced by composition and temperature. The study of recent magnetic and structural properties [19] by substituting chromium atoms by manganese atoms showed a compensation of magnetisation under the effect of composition and temperature. They also showed that there was a composition-dependent structural transformation.

Based on the density functional theory DFT, few calculations of $CoCr_2O_4$ [20, 21] and $CoFe_2O_4$ [22–24] have provided important results concerning the interrelationship between the magnetic and structural properties as well as the sublattice occupations in spinel oxides which are directly linked by their electronic structures.

The control of magnetic polarisation by an electric field or vice versa is ensured through the use of these materials giving rise to many technological devices, such as capacitors, sensors and magnetoelectric memories [25, 26].

In the present work, a methodical analysis of CoX_2O_4 ($X = Cr$, Mn and Fe) spinels based on the study of commonalities as well as differences via structural, electronic, magnetic and optical properties through the use of density functional theory (DFT). We presented a detailed study on the fundamental structural parameters, electronic structure, crystal field variations and their effect on magnetic properties, in addition to an in-depth optical study of these three compounds. The paper is organised as follows: Section 2 presents computational details, Section 3 provides an analysis of the results, followed by conclusions.

2. Calculation details

The use of Wien2k code [27] allowed us to realise the full potential linearised augmented plane wave (FP-LAPW) method. The exchange and correlation potential is treated with the PBE-generalised gradient approximation (GGA) [28]. No approximation of the shape of the potential is made as the cut-off potential extends to 12. The cut-off for the plane wave density is set to $R_{M.T}{*}K_{Max} = 9.5$. For all compounds, $R_{M.T}$ is chosen between 1.85 and 1.9 atomic units (a.u.) for *Co*, *Cr, Mn and Fe* atoms. An 900 *k-points* was chosen to allow integration in their reducible part of the *Brillouin Zone*. When the charge difference is less than 1 mRy, convergence is achieved.

Hamiltonian-type models (e.g. Mott-Hubbard or Anderson's impurity model) seem to be a more natural voice for dealing with highly correlated systems. The Mott-Hubbard model explicitly expresses the opposition between kinetic energy (which depends on the bandwidth defined by the jump integral t) and Coulomb repulsion U between electrons belonging to the same atom. The GGA + U method presented in this section is a combination of the GGA approximation and this model: a correction is made locally, only on the d orbitals in the case in question, by introducing a Hubbard type term $\frac{1}{2}\left(U\sum_{i\neq j} n_i\, n_j\right)$ Hubbard Hamiltonian's form [29] is given by the following expression:

$$H = -t\left(\sum_{\langle i,j\rangle,\sigma} c_{ij}^{\dagger}\, c_{j\sigma}\right) + U\sum n_{i\uparrow} n_{i\downarrow} \tag{1}$$

where $n_{i\sigma} = c_{ij}^{\dagger} c_{j\sigma}$ and $c_{ij}^{\dagger}$ ($c_{j\sigma}$) creates (annihilates) an electron on site i with spin $\sigma = \uparrow$ or $\downarrow$. A nearest neighbour is denoted by $\langle i, j \rangle$. U is the onsite Coulomb repulsion between two electrons on the same site. To allow particles to hop to adjacent sites, hybridisation results between nearest neighbouring orbitals designated by t. Since the atoms are integrated in a polarisable environment, an energy U is needed to move an electron from one atom to another far away. This energy is given by the subtraction between the ionisation potential E_I and the electron affinity E_A. The lowering of the ground state energy of the (N-1) is due to the polarisation of the environment caused by the removal of an electron from a site [30, 31]. Thus,

$$\begin{cases} E_I = E^{(N-1)} - E^{(N)} \text{ and } E_A = E^{(N)} - E^{(N+1)} \\ U = E_I - E_A = (E^{(N-1)} - E^{(N)}) - (E^{(N)} - E^{(N+1)}) = E^{(N+1)} + E^{(N-1)} - 2E^{(N)} \end{cases} \tag{2}$$

where $E^{(N \pm 1)}$ are the ground state energy of $(N \pm 1)$ electron system.

Some work has also been done to try to calculate the value of the effective Coulomb interaction $U_{eff} = (U\text{-}J)$ and J the Hund's coupling. According to Herring [32] U_{eff} could be defined, taking the example of two atoms with n *3d* electrons, as the energy cost of transferring a *3d* electron from one of these atoms to the other

$$2(d^n) = d^{n+1} + d^{n-1} \tag{3}$$

This expression can be complicated if we take into account the screening of other electrons (*4s*, *4p*) and the fact that the number of *4s* electrons can vary if we go from n to (n+1) or (n−1) *3d* electrons. Herring [32] concluded that inside the Wigner–Seitz sphere, the change in the number of *3d* electrons is perfectly screened by a change in the number of *4s* or *4p* electrons of opposite sign. The reaction thus produced is defined by the following equation:

$$2(d^n s^1) = d^{n+1} s^0 + d^{n-1} s^2 \tag{4}$$

The equations (2) and (3) that define U_{eff} lead to the equation proposed by Anisimov et al. [33] and Gunnarsson et al. [34]. This equation calculates the value of the effective Coulomb interaction U_{eff}. The equation (4) also takes into account the variation of the *Fermi* level which occurs in the case of a finite cell. This computation is carried out in the constrained GGA approximation and following the method proposed by Gunnarsson et *al.* [34].

The occupation of the orbits of each atom is well controlled; we build 8-unit supercell whose central atom is considered as an impurity with for occupation of the orbitals $\left(n_{3d\uparrow} = \frac{n}{2} + \frac{1}{2}, n_{3d\downarrow} = \frac{n}{2}\right)$; the other atoms are occupied by orbitals $\left(n_{3d\uparrow} = \frac{n}{2} + \frac{1}{2}, n_{3d\downarrow} = \frac{n}{2} - 1\right)$ and in order to allow all the electrons

to contribute to the filtering, for each configuration self-consistent potentials are determined. The Slater transition rule [35] allows the following equation to be obtained

$$U_{eff} = \begin{cases} \varepsilon_{3d\uparrow}\left[n_{3d\uparrow} = \frac{n}{2}+\frac{1}{2}, n_{3d\downarrow} = \frac{n}{2}\right] - \varepsilon_{3d\downarrow}\left[n_{3d\uparrow} = \frac{n}{2}+\frac{1}{2}, n_{3d\downarrow} = \frac{n}{2}-1\right] \\ -\varepsilon_{F}\left[n_{3d\uparrow} = \frac{n}{2}+\frac{1}{2}, n_{3d\downarrow} = \frac{n}{2}\right] + \varepsilon_{F}\left[n_{3d\uparrow} = \frac{n}{2}+\frac{1}{2}, n_{3d\downarrow} = \frac{n}{2}-1\right] \end{cases} \quad (4)$$

where $\varepsilon_{3d\uparrow}$ and $\varepsilon_{3d\downarrow}$ are the *3d* eigenvalues at the central atom calculated at the fixed occupancies. In Ref. [31] we argue that we should use this value for U and set J to zero. The calculated values of U_{eff} Wien2k code [27] are: $U(Co) = 3.389$ eV and $U(Cr) = 1.383$ eV for $CoCr_2O_4$, $U(Fe) = 3.371$ eV and $U(Co) = 3.292$ eV for $CoFe_2O_4$, $U(Co) = 3.968$ and $U(Mn) = 3.417$ eV for $CoMn_2O_4$.

3. Results and discussions

3.1. The crystalline structure of spinel

The spinel structure is generally a cubic structure with a space group $Fd\bar{3}m$ having two types of cation in the sub-lattice *A* and *B* with tetrahedral and octahedral symmetry respectively. Cations *A* and *B* are in the +2 and +3 state respectively (Figure 1). A spinel formula unit consists of one sub-lattice *A* and two sub-lattice *B*. When *B* cations occupy the tetrahedral sites leading to the displacement of *A* cations to the octahedral sites, in this case we speak of the inverse spinel structure. In our case the oxide $CoFe_2O_4$ has an inverse spinel structure without distortion [36] while for the spinel $CoMn_2O_4$, it has a body-centred tetragonal structure with a space group $I4_1/amd$ [37] but always with a spinel structure. Finally, for the third material $CoCr_2O_4$ we have a normal spinel structure [38]. It should be recognised that in $CoFe_2O_4$ its insulating or semi-metallic ground state is linked by the occupation of these sub-lattices [22, 23]. Experimental work using neutron diffraction has confirmed that the two compounds $CoCr_2O_4$ and $CoMn_2O_4$ with inclined magnetic spin structures [9, 37] on the other hand the oxide $CoFe_2O_4$ is in the collinear ferrimagnetic state. According to *Neel*'s configuration [36], the magnetic moments of cations *A* and *B* are anti-aligning. This was later confirmed by the studies of Mössbauer [39]. Experimentally, according to the occupation of the sub-lattices, the two spinels $CoCr_2O_4$ and $CoMn_2O_4$ have been considered as normal spinel. In the case of $CoFe_2O_4$, the sub-lattices adapt the inverse spinel structure, taking into account a maximum inversion. and cobalt and iron atoms have a high spin configuration whether in octahedral or tetrahedral sites in partial reverse spinels [23]. In order to reassure the modelling of the disorder of the sub-lattices we need either to take into account the averaging

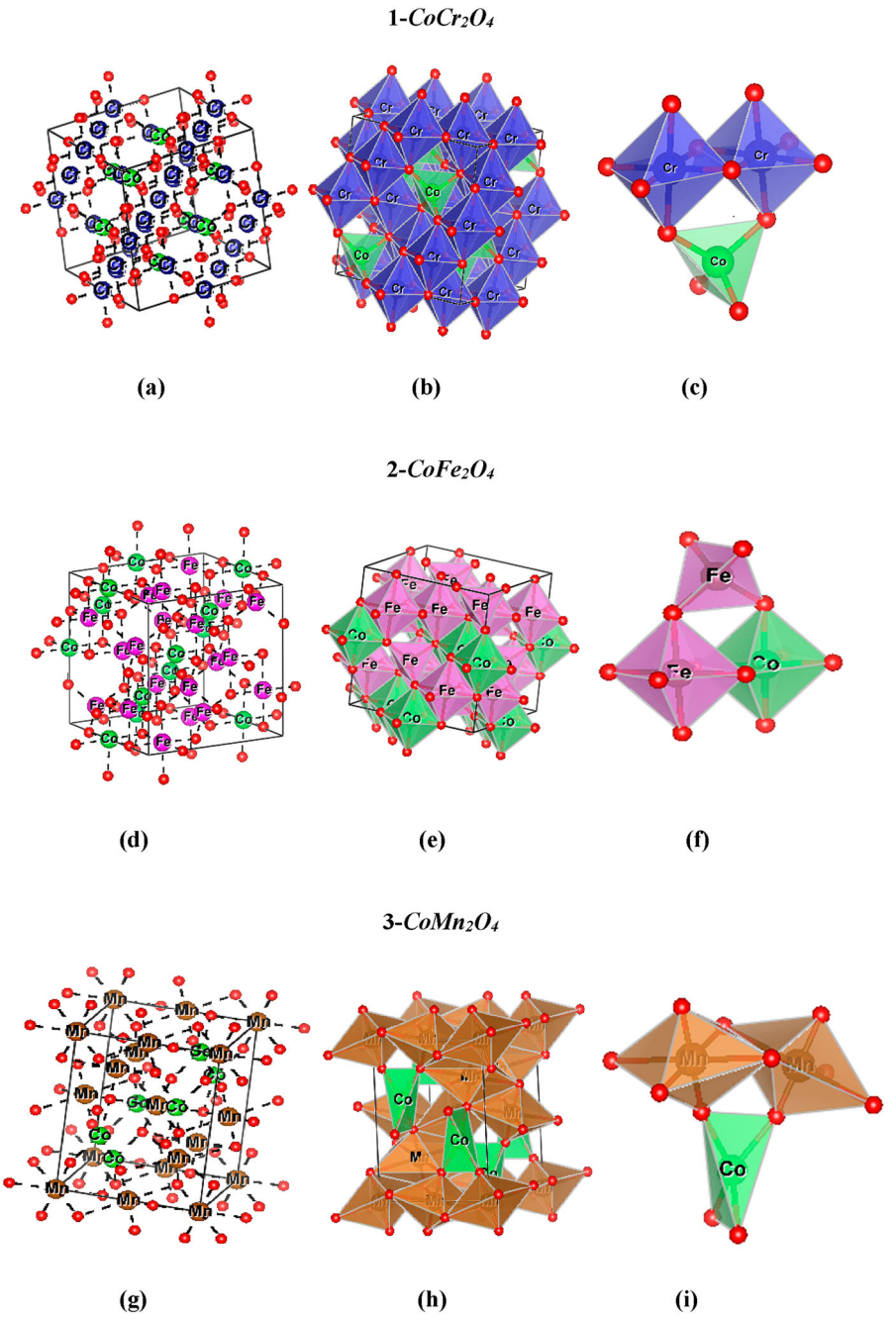

Figure 1. The crystalline structure of CoX_2O_4 ($X = Cr$, *Mn* and *Fe*), the octahedral and tetrahedral sites in normal (a)–(c) ((g)–(i)) $CoCr_2O_4$ ($CoMn_2O_4$) spinel and inverse spinel (d)–(f) $CoFe_2O_4$ structure. *Cr*: blue, *Fe*: purple, *Mn*: brown, *Co*: green, *O*: red.

procedure of the mean field configuration [24], or the construction of a supercell in the current approach, in our case we have considered the inverse spinel type structure [22]. In the theoretical work [40], they assumed that all three

compounds have collinear magnetic configurations despite the fact that the $CoCr_2O_4$ and $CoMn_2O_4$ compounds are not. Their choices were justified by the fact that collinear magnetic states add important qualitative information. Concerning ferrite cobalt and chromium cobalt, they found that the *Neel* configuration had the lowest energy. For the $CoMn_2O_4$ spinel, the magnetic moments at the sites of a sub-lattices are antiparallel, this implies that the total magnetic moment is zero. They found that in the case of the *Neel* configuration the energy was only about 1 meV per atom higher, this clearly tells us that the magnetic state of magnesium cobalt was frustrated. So they took into account only the configuration of *Neel*. In our work we have only considered the *Neel* configuration, we assumed that all three compounds have collinear magnetic configurations.

3.2. Structural properties

All three compounds have a ferrimagnetic configuration. The atomic positions are minimised using the approach of Hellmann–Feynman forces as well as the total energy of the unit cell, the relaxed positions are summarised in Table 1 using GGA + U approximation for the three spinel's. Our results agree well with the experimental work [36, 37, 41]. The ground state is obtained by calculating the total energy at different volumes then the results are fitted using the Murnaghan equation of state (EOS) [42] with two approximations GGA and GGA + U (see Figure 2).

The optimised parameters calculated with GGA and GGA + U at equilibrium such as lattice parameter, minimum energy and compressibility modulus are collected in Table 2. Our lattice parameters calculated with GGA + U agree well with the theoretical and experimental values. To date, the experimental

Table 1. Fractional atomic coordinates of $CoCr_2O_4$, $CoMn_2O_4$ and $CoFe_2O_4$ with GGA + U approximation.

Compounds	Atomic positions (fractional coordinates)
$CoCr_2O_4$	*Co*: (0.125,0.125, 0.125) *Cr*: (0.5, 0.5, 0.5) *O*: (0.2611, 0.261, 0.261) (0.262, 0.262,0.262) DFT + U [40] (0.264, 0.264,0.264) EXP [41]
$CoMn_2O_4$	*Co*: (0.5, 0.25, 0.125) *Mn*: (0.25, 0.75, 0.25) *O*: (0.24, 0.25, 0.256) (0.255, 0.255,0.267) DFT + U [40] (0.230, 0.230, 256) EXP [37]
$CoFe_2O_4$	*Co*: (0.125,0.125, 0.125) *Fe*: (0.5, 0.5, 0.5) *O*: (0.256, 0.256, 0.256) (0.255, 0.255, 0.255) DFT + U [40] (0.256,0.256, 0.256) EXP [36]

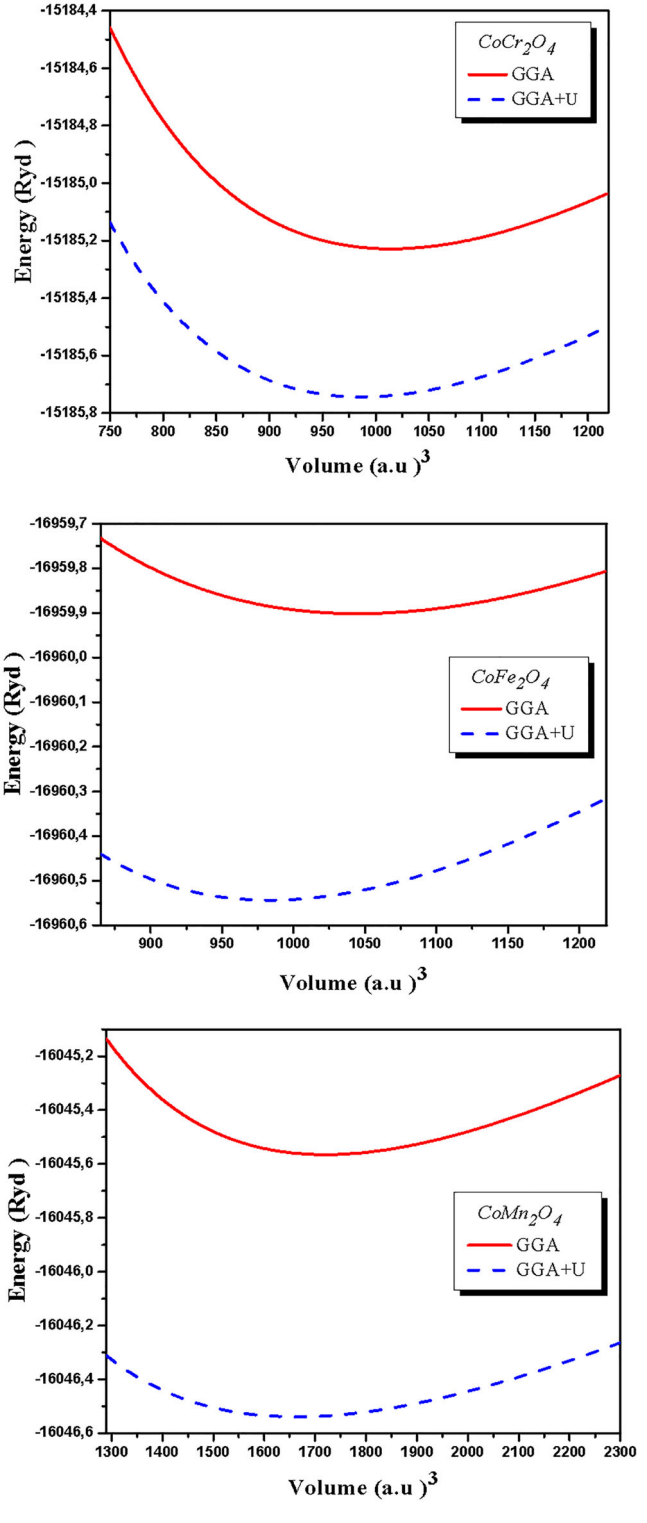

Figure 2. Comparison between the total energies as a function of the volume of the spinels $CoCr_2O_4$, $CoMn_2O_4$ and $CoFe_2O_4$ with the GGA and GGA + U approximations.

modulus of compressibility is not yet known, but previous tests predict that their compressibility modulus is between 180 and 200 GPa [43].

Our compressibility moduli are between $B = 180$ and 195 GPa (see Table 2) this is in agreement with the previously reported experimental values [43]. Details of the different bond lengths and angles of the different octahedral and tetrahedral sites are presented in Table 3.

$CoFe_2O_4$ and $CoCr_2O_4$ are spinel structured and crystallises in the cubic $Fd\bar{3}m$ space group. These structures are three-dimensional. *Fe* (*Cr*) is bonded to six equivalent *O* atoms to form FeO_6 (CrO_6) octahedra that share corners with six equivalent CoO_4 tetrahedra and edges with six equivalent FeO_6 (CrO_6) octahedra. All Fe_T–*O* (*Cr–O*) bond lengths are 1.9 Å (2.020 Å). *Co* is bonded to four equivalent *O* atoms to form CoO_4 tetrahedra that share corners with twelve equivalent FeO_6 (CrO_6) octahedra. The corner-sharing octahedral tilt angles are 57° (59°). All *Co–O* bond lengths are 2.063 Å (1.99 Å). *O* is bonded to three equivalent *Fe* (*Cr*) and one *Co* atom to form a mixture of distorted edge and corner-sharing OFe_3Co (OCr_3Co) trigonal pyramids.

The tetrahedral sites of the stable cubic phase of $CoCr_2O_4$ are almost without any local distortion as shown by the ideal value of the *O-Co-O* angles of 109.47°. On the other hand, octahedral sites are slightly locally distorted since the

Table 2. Theoretical and experimental structural data using GGA and GGA + U of $CoCr_2O_4$, $CoMn_2O_4$ and $CoFe_2O_4$ spinels.

Compounds	The parameters	GGA	GGA + U
$CoCr_2O_4$	a (Å)	8.36	8.44
			DFT + U: 8.35 [40], EXP: 8.34 [41]
	$\left.\frac{\Delta a}{a}\right\|_{Exp}$	0.23	1.18
	B (GPa)	189.31	188.03
	B'	4.29	4.23
	V_0 (Å)^3	584.61	601.21
	E_{min} (Ry)	−15185.743982	−15185.228473
$CoFe_2O_4$	a (Å)	8.352	8.552
			DFT + U: 8.41[40], EXP: 8.366 [36]
	$\left.\frac{\Delta a}{a}\right\|_{Exp}$	−0.16	2.17
	B (GPa)	180.89	182.92
	B'	4.24	4.15
	V_0 (Å)^3	582.70	625.40
	E_{min} (Ry)	−16960.543766	−16959.936498
$CoMn_2O_4$	a (Å)	8.09	8.16
			DFT + U: 8.17 [40], EXP: 8.1 [37, 41]
	$\left.\frac{\Delta a}{a}\right\|_{Exp}$	−0.12	0.7
	c (Å)	9.15	9.36
			DFT + U: 9.39 [40], EXP: 9.13 [37], 9.3 [41]
	$\left.\frac{\Delta c}{c}\right\|_{Exp}$	0.21[37], −1.63[41]	2.45 [37], 0.64 [41]
	c/a (Å)	1.13	1.14
	B (GPa)	189.31	195.14
	B'	4.29	5
	V_0 (Å)^3	584,61	1719.08
	E_{min} (Ry)	−16046.539172	−16045.564902

Table 3. Interatomic distances (in Å) and angles (in deg) of the spinels $CoCr_2O_4$, $CoMn_2O_4$ and $CoFe_2O_4$ within GGA and GGA + U approximations.

Spinels	Interatomic distances and angles	GGA	GGA + U
$CoCr_2O_4$	*Co-Cr (×2)*	3.46	3.499, 3.46 [40]
	Co-O (×4)	1.97	1.99, 1.97 [40]
	Cr-Cr (×1)	2.95	2.98, 2.95 [40]
	Cr-O (×6)	2.001	2.02, 2.00 [40]
	O-Cr-O	84.53	84.53, 84.55 [40]
		95.47	95.468
	O-Co-O	109.47	109.47, 109.47 [40]
	Cr-O-Cr	95.22	95.22, 121.53 [40]
$CoFe_2O_4$	*Co-Fe* (×2)	2.85	2.98, 2.99 [40]
		3.33	3.50, 3.50 ± 0.02 [40]
	Co-O (×6)	2.06	2.0636
			2.09 ± 0.03(×6) [40]
	Fe-Fe (×1)	3.36	3.504, 3.53 ± 0.07 [40]
	Fe-O (×2) Tetra	1.90	1.9178
	Fe-O (×2) Tetra	1.86	1.9179
	Fe-O (×6) Octa	1.99	1.90 ± 0.01 [40]
			2.063, 2.03 ± 0.01 [40]
	O-Fe-O (×2) Octa	82.63	87.15
	O-Fe-O (×4) Octa	92.34	92.85
	O-Fe-O (×4) Tetra	109.35	109.47
			90.24 ± 0.07 [40]
	O-Co-O Octa	83.07 (×2)	92.85 (×4)
		88.42(×2)	87.15 (×4)
		91.43 (×2)	88.23 ± 20 [40]
		96.93(×2)	
	Fe-O-Fe	118.51	121.27
			121.53 [40]
	Fe-O-Co (×1)	125.89	123.27
			124.16 [40]
$CoMn_2O_4$	*Co-Mn* (×2)	4.07	3.97, 3.55 ± 0.15 [40]
	Co-O (×4)	2.33	2.24, 1.99 [40]
	Mn –Mn (×1)	4.08	3.70, 3.03 ± 0.15 [40]
	Mn–O (×2)	1.79	1.77
	Mn–O (×4)	3.42	3.11
			2.07 ± 0.22 [40]
	O-Mn-O	88.71, 91.28, 102.11	78.45, 89.15, 90.84, 101.54
			85.58 ± 0.94 [40]
	O-Co-O	75.56, 128.65	70.33, 131.93, 108.14 ± 4.13 [40]
	Mn-O-Mn	73.39	73.05, 122.2 ± 4.13° [40]

O-Cr-O angle is 84.53° deviating from the ideal value of 90°. In addition, the value of the *Co-O-Cr* angle is 121.53° which deviates from the ideal value of 125°.

On the other hand, the tetragonal phase of $CoMn_2O_4$ with the ratio between these lattice parameters equal to $c/a = 1.14$ creates different angles and atomic distances which are substantially dispersed (see Table 3). *Mn* is bonded to six equivalent *O* atoms to form MnO_6 octahedra that share corners with six equivalent CoO_4 tetrahedra and edges with six equivalent MnO_6 octahedra. There are two shorter (1.76 Å) and four longer (3.11 Å) *Mn–O* bond lengths. *Co* is bonded to four equivalent *O* atoms to form CoO_4 tetrahedra that share corners with twelve equivalent MnO_6 octahedra. The corner-sharing octahedra tilt angles range from 55 to 59°. All *Co–O* bond lengths are 2.24 Å. *O* is bonded in a rectangular see-saw-like geometry to three equivalent *Mn* and one *Co* atom.

At the tetrahedral sites, the *O-Co-O* bond angles are 70.33, 131.93 indicating substantial distortion. The *Mn-O* bonds elongate (contract) along the directions *z*(*xy*) resulting in considerable deformation at the octahedral level. This varies the angles *O-Mn-O* and *Mn-O-Co*.

Since the z-axis elongates by 0.5%, the real cubic structure of cobalt ferrite deviates from the perfect structure. This is due to the slight deformation of the octahedrons around the *Co* and *Fe* sites. So, along the *z*-direction there is a slight lengthening of the *Co-O* bonds, while in the *xy* plane the *Fe-O* bonds contract giving rise to a small tetragonality. The deformations are due to the cobalt atoms in the octahedral sites this is confirmed by the angles at the octahedral and tetrahedral sites. *O-Fe-O* is 92.85. This value is very close to the ideal value of the 90° spinel structure, while the *O-Co-O* angle is 87.14. On the other hand, *CoO-O-FeT* (*FeO-O-FeT*) is 121.272° (123.272°) deviating from the ideal spinel value of 125°.

Trends observed in the structural aspects of CoX_2O_4 ($X = Cr$, Mn and Fe) compounds can be explained this is achieved through an analysis of the electronic configurations of the energy levels of the cations in the tetrahedral and octahedral sites. In the case of the Cr^{3+} octahedra of the $CoCr_2O_4$ spinel, the higher lying e_g states are empty on the other side, the Mn^{+3} octahedra have the $(e_g)^1$ configuration. At this level and in the compound $CoMn_2O_4$, there is degeneration. In order to lift this degeneration there will be a lowering in the symmetry of the crystalline structure inducing the tetragonal ground state. The understanding of the magnitude of the tetragonal distortion is explained by Dunitz and Orgel [44] on the configuration of $Mn^{3+}(t_{2g})^3$ $(e_g)^1$ ions. The t_{2g} orbitals of the Co^{2+} ions in the $CoFe_2O_4$ spinel are degenerated leading to a lowering of the cubic symmetry. The understanding of the low value of the distortion is based on the $(t_{2g})^5$ $(e_g)^2$ configuration of the orbital of the cobalt atom in the octahedral sites [43]. Concerning the Iron atoms in the tetrahedral sites the configuration is given by $(e_g)^2$ $(t_{2g})^3$ but in the octahedral sites the image is inverted giving rise to a configuration $(t_{2g})^3$ $(e_g)^2$.

It was found that the chemical bonds between *X* cations and oxygen atoms decreased when iron atoms were replaced with chromium and then manganese atoms. Concerning the angles between the cobalt atoms and the oxygen atoms, they increase when changing from $CoFe_2O_4$ to $CoCr_2O_4$ to $CoMn_2O_4$. The angles between the cations *X* and *O* decrease from $CoMn_2O_4$ to $CoFe_2O_4$ to $CoCr_2O_4$.

3.3. Electronic and magnetic properties

The determination of the electronic and magnetic properties of spinels is based on the understanding of the electron configuration of the *d*-orbital of cations in the tetrahedral and octahedral sites. According to crystal field theory [45], the interplay between the intra-atomic exchange field (*EX*) and the relative

strengths of the crystal field (*CF*) determines the electron configuration. In order to better understand the electronic and magnetic properties of our compounds, with the help of an analysis of the total and partial electronic density we will study the exchange splitting and the relative forces of the crystalline field splitting while trying to make a link between the electronic properties and structural distortions of CoX_2O_4 ($X = Cr$, Mn and Fe) spinels. In tetrahedral sites, the t_{2g} levels are higher than the e_g levels. This is explained by the direct electrostatic repulsive interaction between the anionic and t_{2g} orbitals. On the other hand, in the octahedral sites, there is a reversal of order due to repulsion in the e_g orbitals. When $c/a > 1$, in the case of the tetragonal distortion: In octahedral sites, there is a splitting into two levels of e_g. The first level is that of the d_z^2 orbital with an energy lower than the second level d_{xy}^2. While the splitting of the t_{2g} level leads to two levels: the first $d_{zy}(d_{zx})$ is lower doubly degenerate and the second higher level is d_{xy}. The intensity of the exchange and crystal fields determines the spacing of these energy levels. The bandgap of semiconductor materials is influenced by the result of the competition between the (CF) division and (EX) division. In the case of $CoCr_2O_4$, an exchange splitting and a crystal field splitting at the chromium site, both equally strong, determine the gap. In the case of $CoMn_2O_4$ and $CoFe_2O_4$, the exchange splitting at the X sites is stronger than the crystal field splitting. This will cause the gap to increase from *Fe* to *Mn* and then *Cr* (see Table 4).

In order to produce the correct semiconductor states, the electron–electron correlation effect was introduced by the GGA + U approximation. This can be achieved by integrating the appropriate localisation of the states while breaking down the degeneracy in the X cation orbits in CoX_2O_4.

We have shown the band structure of CoX_2O_4 ($X = Cr$, Mn and Fe) compounds in Figure 3. From the graphs, the gap between the valence and conduction bands is calculated within GGA + U to be between 0.68 and 2.82 eV for spin down which gives CoX_2O_4 ($X = Cr$, Mn and Fe) compounds the property of being a semiconducting material. The band structure of Fe_2CoO_4 (Mn_2CoO_4) and Cr_2CoO_4 shows a direct band gap at the Γ point and k point respectively.

The total and partial density of states calculated using GGA + U approximation are shown in Figure 4. It has been noticed that for the $CoCr_2O_4$

Table 4. The Hubbard parameter as well as the energy gap E_g of the three compounds $CoCr_2O_4$, $CoMn_2O_4$ and $CoFe_2O_4$ calculated in the approximations GGA and GGA + U.

			E_g (eV)	
Spinel	The Hubbard parameters (eV)	Spins	GGA	GGA + U
$CoCr_2O_4$	$U(Co) = 3.389$	Up	1.027	1.95
	$U(Cr) = 1.383$	Down	1.88	2.82
$CoFe_2O_4$	$U(Fe) = 3.371$	Up	1.423	2.00
	$U(Co) = 3.292$	Down	0.06	0.68
$CoMn_2O_4$	$U(Co) = 3.968$	Up	0.63	1.25
	$U(Mn) = 3.417$	Down	1.19	2.47

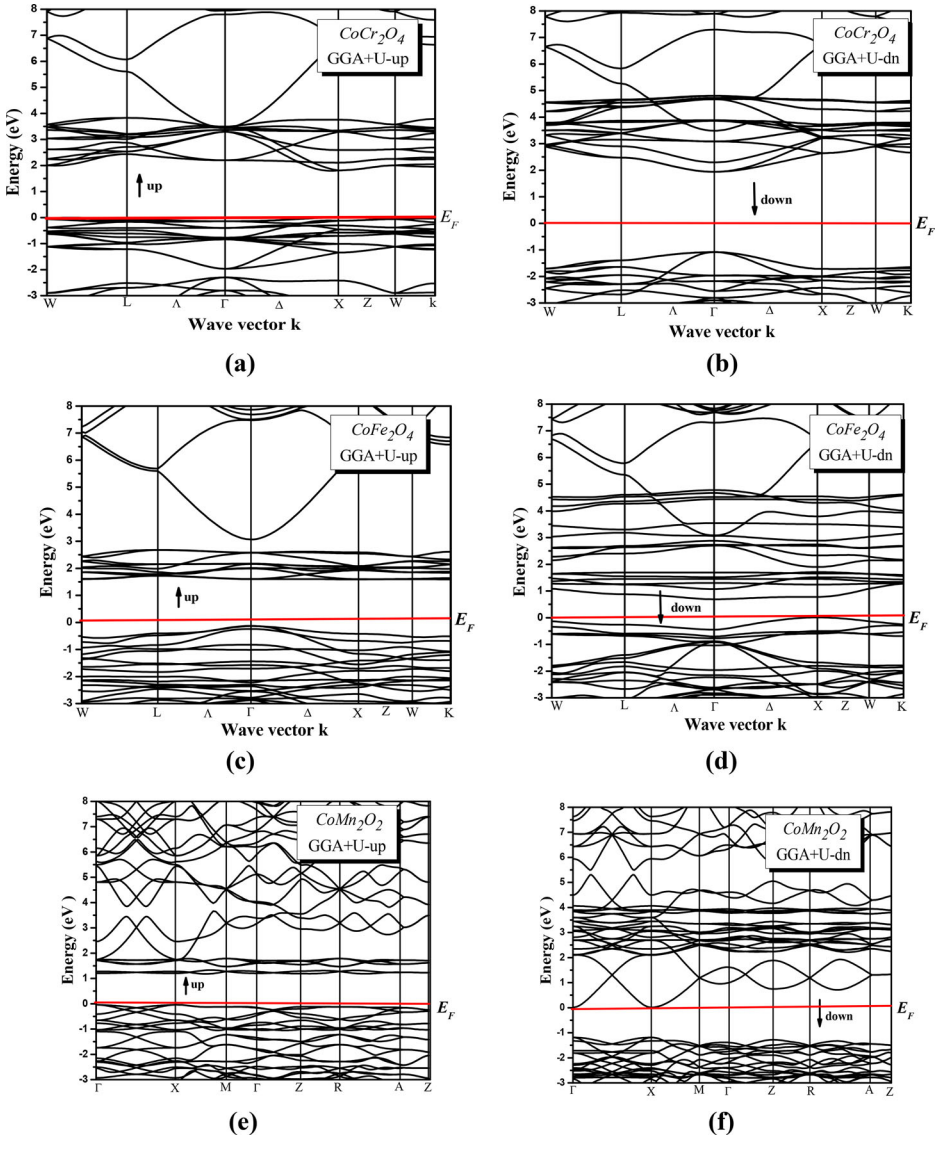

Figure 3. Electronic band structure for CoX_2O_4 ($X = Cr$, Mn and Fe) spinels.

spinel around −2 eV (−6 eV) the $t_{2g}^{\downarrow}$ ($e_g^{\downarrow}$) of the cobalt atom are localised. For the minority spins, the *p* states of *O* are hybridised mainly with the e_g states. For the majority spins the cobalt t_{2g} states are centred around 2–4 eV so they are unoccupied. However, the two electrons of the e_g states are localised between −1 eV and −2 eV. This gives rise to a magnetic moment of about 3 μB for the cobalt atom (Table 4). Concerning the chromium atom, the t_{2g} states are not influenced by the incorporation of the strong correlation, it was noticed that for the majority spins near the *Fermi* level these states are always fully occupied by the localised electrons. On the other hand, for the minority spins the t_{2g}

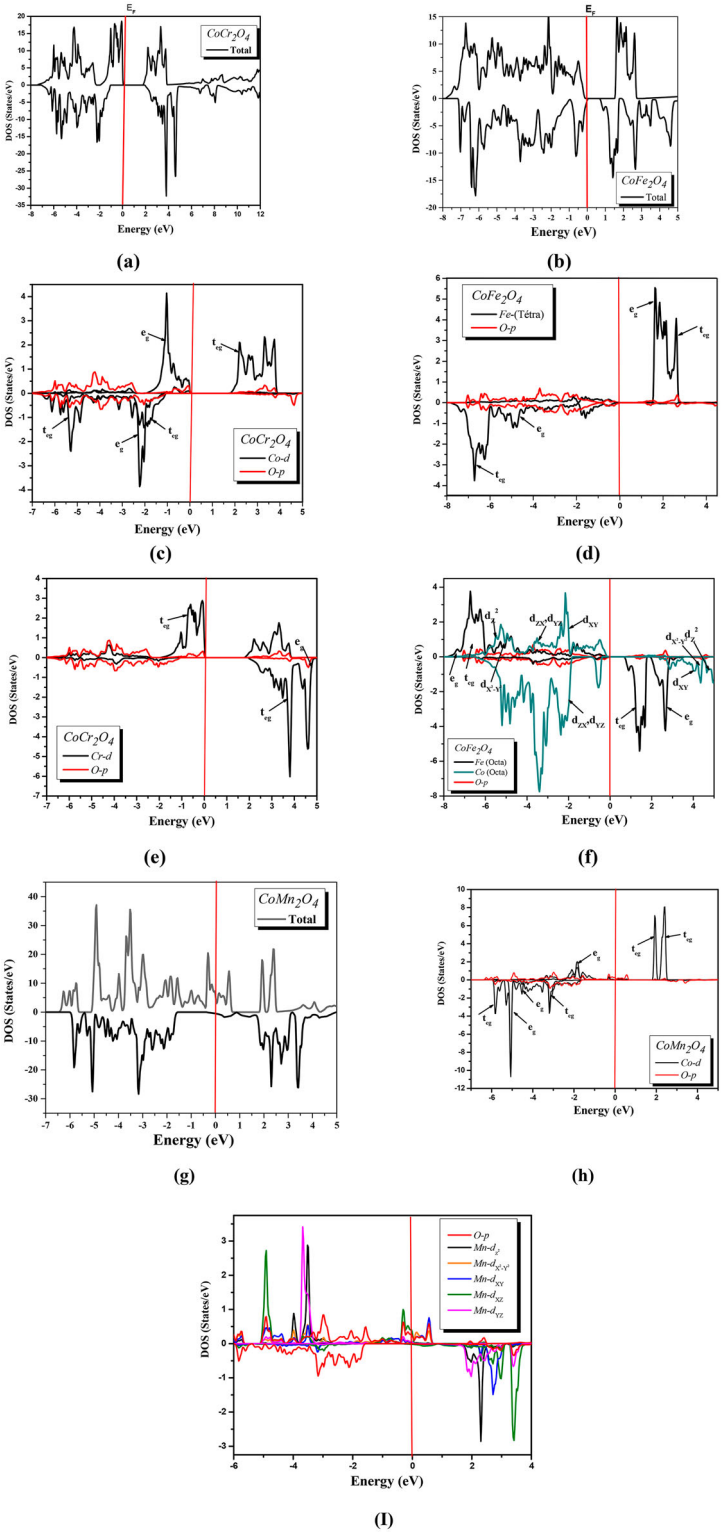

Figure 4. The calculated total and partial density of states for $CoCr_2O_4$, $CoMn_2O_4$ and $CoFe_2O_4$ spinel compounds.

states which are not occupied are pushed towards higher energies. There is a weak hybridisation between these states and oxygen atoms, which gives rise to a magnetic moment equal to 3 μB for chromium atoms as well, but with a sign opposite to that of cobalt atoms, (see Table 4).

The t_{2g} states of the cobalt atom in the $CoMn_2O_4$ spinel are similar to those of $CoCr_2O_4$, except that the energy is shifted to a lower energy. There is a strong hybridisation between the oxygen atoms and the cobalt states compared to the $CoCr_2O_4$ spinel because the cobalt states are more delocalised giving rise to a magnetic moment of 3μB of cobalt just like $CoCr_2O_4$. The large tetragonal distortion leads to the degeneration of the *d* states which is lifted from the manganese, which means that the state densities of the *Mn* site are more interesting. Based on crystal field theory: The high-energy e_g states are divided into d_z^2 and $d_{\bar{x}^{22}_{-y}}$ states. The d_z^2 states are occupied and d_{xy}^2 participate in the formation of covalent bonds with oxygen [46]. This phenomenon is confirmed in the case of the minority spins in Figure 4. There are distinct peaks at about −6 eV and at about 1 eV due to the half-filled $d_z^{2\uparrow}$ states. There is a hybridisation between the $d_{xy}^{2\uparrow}$ states and the *p* states of oxygen allowing the states to be more localised. The magnetic moment of *Mn* is close to 4 μB because the minority spins are almost empty (Table 4). The t_{2g} states are more delocalised compared to the case where the effect of the electron–electron correlation was absent and the lifting of degeneracy has less effect. The additional electron of magnesium compared to chrome leading to states close to the *Fermi* level, which reduces the band gap of $CoMn_2O_4$ (2.467 eV) compared to $CoCr_2O_4$ (2.818 eV).

The inverted structure of the $CoFe_2O_4$ spinel implies different occupations of the sub-lattices introducing qualitatively different density of state of *A* and *X* sites (Figure 4). The unoccupied states of the majority spins are pushed towards higher energy due to the introduction of strong correlations. We have a small hybridisation, in the minority spin band, between electrons which are extremely localised around −6 eV to −7 eV and oxygen states. Then the iron atoms in the tetrahedral sites have a moment of 4 μB. There are two types of atoms: iron atoms and cobalt atoms in octahedral sites. Then the states associated with these two atoms have qualitatively very different characteristics. For both atoms the minority spins the $e_g^{\downarrow}$ states are completely empty. The t_{2g} band of iron atoms in the octahedral sites is completely full and is extremely localised around −6 eV to −7 eV. Then in the spinel, $CoFe_2O_4$ the *Fe* states are localised whatever the crystalline environment. On the other hand, in the spin up band, the cobalt states in the octahedral sites are delocalised. Despite the distortions associated with the octahedral cobalt sites, the t_{2g} degeneration is broken only slightly. We have peaks close to the *Fermi* level around −1 eV this is due to the d_{zx}, d_{yx} states in the spin down band. This phenomenon was not present for the other compounds in the states associated with octahedral sites. These states are due to the extra electrons

in iron, compared to chromium and manganese. This leads to a smaller energy gap compared to $CoCr_2O_4$. The gap calculated using GGA + U is 2 eV. In the spin up band the t_{2g} states of cobalt are delocalised, hybridising with the p states of oxygen. Then the magnetic moments are about 3 and 4 μB for cobalt and iron in the octahedral sites of the $CoFe_2O_4$ spinel, (Table 5).

3.4. Optical properties

Using the approximation GGA + U we have calculated the different optical properties such as the imaginary parts $\varepsilon_2(\omega)$ of the dielectric function $\varepsilon(\omega) = \varepsilon_1(\omega) + i\varepsilon_2(\omega)$ for an energy range from 0 to 30 eV (Figure 5(a)). The transitions between each pair of occupied and unoccupied bands determine the imaginary part of the dielectric function. Then the origin of each peak can be determined from the contribution of each electronic transition from an occupied valence state to an empty conduction state. The optical spectra come from the upper valence bands to the lower conduction bands. According to Figure 5(a), the spectra of the imaginary part of the three spinels are almost the same. The optical absorption edge is the first critical point to determine which is the division between the valence bands (*VB*) and

Table 5. The theoretical magnetic moments values (m_0) calculated for the spinels CoX_2O_4 (X = *Cr*, *Mn* and *Fe*) using GGA, GGA + U approximations.

The spinels	The moment *m*0 (μB/f. u)*m*0(μB/f. u)	GGA	GGA + U
$CoCr_2O_4$	Interstitial	1.67	1.64
	Co (Tetra)	−2.33	−2.53
			−2.66 [40]
	Cr (Octa)	2.34	2.42
			2.94 [40]
	O	0.05	0.03
	Total	3.000631	2.997085
			2.95 [40]
$CoFe_2O_4$	Interstitial	0.20	0.024
	Fe (Tetra)	−3.49	−3.74
			−3.98 [40]
	Co (Octa)	2.51	2.60
			2.66 [40]
	Fe (Octa)	3.58	3.87
			4.10 [40]
	O	0.079	0.075
	Total	3.00	2.99999
			2.98 [40]
$CoMn_2O_4$	Interstitial	4.48	4.39
	Co (Tetra)	−2.51	−2.62,
			−2.68 [40]
	Mn (Octa)	3.16	3.82
			3.81 [40]
	O	0.09	−0.08
	Total	6.30	4.90
			4.84 [40]

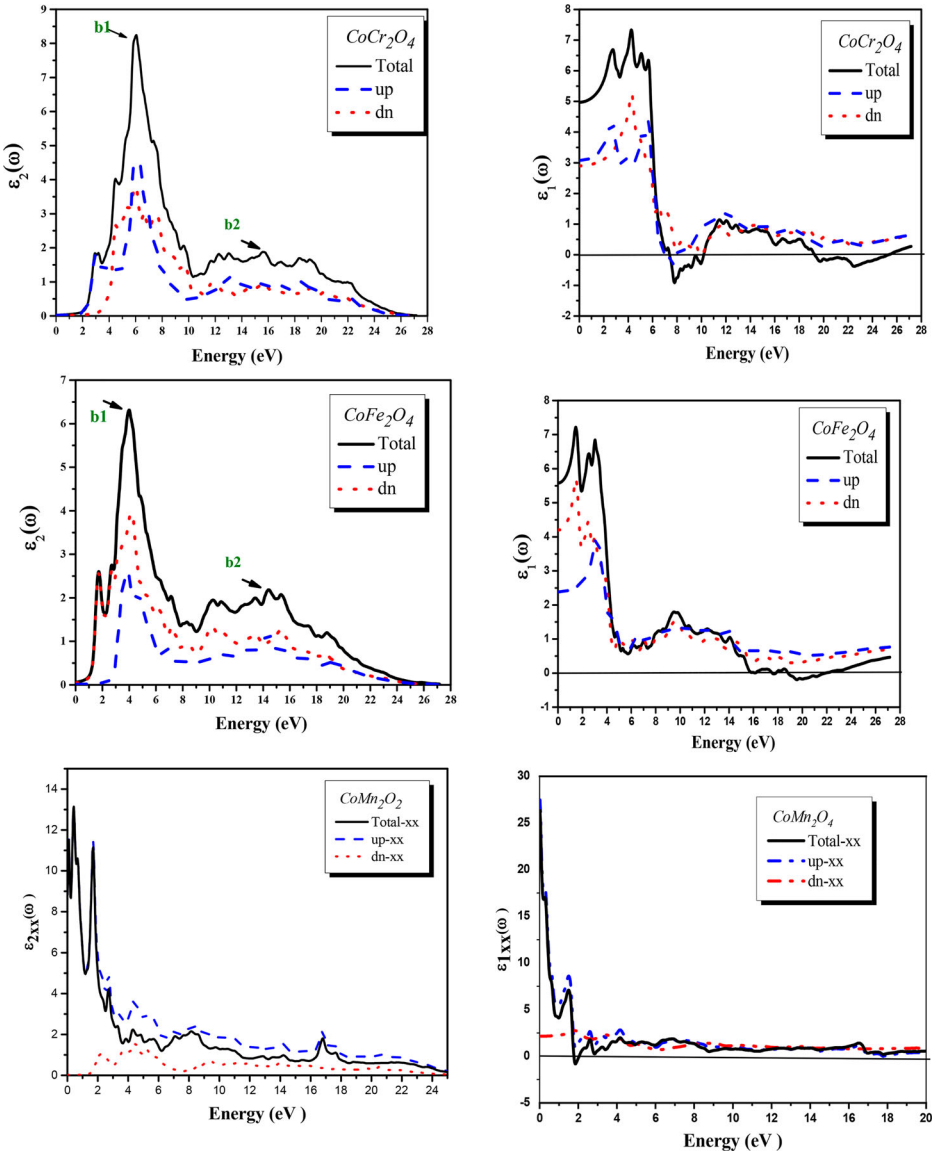

Figure 5. (a) and (b) Variation of the imaginary and real part of the dielectric function respectively, (c) the refractive index and (d) the extinction coefficient, (e) reflectivity spectra, (f) the absorption coefficient, (g) variation of the optical conductivity and (h) the energy loss function as a function of energy for CoX_2O_4 ($X = Cr$, Mn and Fe) within GGA + U approximation.

the conduction bands (*CB*). This will give the threshold of the direct optical transition between the upper *VB* V_1 and the lower *CB* C_1 ($V_1 \rightarrow C_1$ transition); the counting of the bands is done from the bottom (top) of the conduction (valence) band. Otherwise known as the fundamental absorption edge. We have identified two absorption peaks, indicated by b1 and b2, b1 located at the energies: 6.05, 4.1 and 2.10 eV, b2 located at the energies 15.57 eV, 14.46

and 5.29 eV for $CoCr_2O_4$, $CoFe_2O_4$ and $CoMn_2O_4$ respectively. In the ultraviolet region we find the two peaks (b1 and b2) except for b1 of $CoMn_2O_4$ which belongs to the visible region. These peaks are due to the majority state electronic transitions of b1 and the majority and minority state transitions of b2 for $CoCr_2O_4$. For the $CoFe_2O_4$ spinel these peaks are due to the electronic transitions of the minority state and for $CoMn_2O_4$, these peaks are due to the electronic transitions along the *zz* axes of the majority (minority) state of b1 (b2). In the minority state, the absorption maximum of the dielectric function of $CoCr_2O_4$, $CoFe_2O_4$ and $CoMn_2O_4$ occurs at energy 2.97, 1.10 and 3.7 eV, and in the majority state occurs at energy 2.29, 2.51 eV. The spectra of all three compounds move towards a lower energy from $CoCr_2O_4$ to $CoMn_2O_4$ to $CoFe_2O_4$. This is explained by the fact that the value of the band gap decreases when moving from $CoCr_2O_4$ to $CoMn_2O_4$ to $CoFe_2O_4$. Using the Kramers–Kronig relation, we obtained the dispersive parts $\varepsilon_1(\omega)$ of the dielectric functions from the corresponding $\varepsilon_2(\omega)$ of the CoX_2O_4 ($X = Cr$, Mn and Fe) spinels, $\varepsilon_1(\omega)$ are shown in Figure 5(b). The lower energy limit of $\varepsilon_1(\omega)$ gives rise to the static dielectric constant $\varepsilon_1(0)$ *e.i.* $\varepsilon_1(0) = \varepsilon_1(\omega \to 0)$. The values of the $\varepsilon_1(0)$ are collected in Table 6. When the value of the energy gap decreases, the static value $\varepsilon_1(0)$ increases this is in accordance with the Penn model which is based on the following equation $\varepsilon_1(0) \approx 1 + \left(\frac{\hbar\,\omega_P}{E_g}\right)^2$ where $\hbar\,\omega_P$ is the plasma energy; $\varepsilon_1(0)$ is inversely proportional to E_g. Thus, a smaller E_g gives a larger $\varepsilon_1(0)$. We have noticed a large anisotropy in the real part $\varepsilon_1(\omega)$ of dielectric function for the $CoMn_2O_4$ compounds.

Figure 5(c) and (d) shows the evolution of the refractive index $n(\omega)$ and the extinction coefficient $k(\omega)$ with the variation in photon energy for the three spinels. When the energy is low, the refractive index variation remains constant afterwards when approaching the edge of absorption, it starts to increase until it reaches a maximum and then it decreases for a higher energy. The calculated static refractive index $n(0)$ is summarised in the same table with $\varepsilon_1(0)$. The value of $n(0)$ increases when replacing the chromium atom with magnesium

Table 6. ε_1 (0) and n (0) for CoX_2O_4 ($X = Cr$, Mn and Fe) within GGA + U approximation.

The spinels		$\varepsilon_1(0)$			$n(0)$	
$CoCr_2O_4$	Up	3.07		Up		1.75
	Down	2.89		Down		1.75
	Total	4.97		Total		2.23
$CoFe_2O_4$	Up	2.38		Up		1.54
	Down	4.19		Down		2.04
	Total	5.58		Total		2.36
$CoMn_2O_4$	Up	$\varepsilon_{1xx}(0)$	27.48	Up	$n_{xx}(0)$	5.30
		$\varepsilon_{1zz}(0)$	8.83		$n_{zz}(0)$	6.95
	Down	$\varepsilon_{1xx}(0)$	2.14	Down	$n_{xx}(0)$	1.46
		$\varepsilon_{1zz}(0)$	0.01		$n_{zz}(0)$	1.71
	Total	$\varepsilon_{1xx}(0)$	26.33	Total	$n_{xx}(0)$	5.20
		$\varepsilon_{1zz}(0)$	8.82		$n_{zz}(0)$	6.81

and subsequently the iron atom, following a trend opposite to that of the band gap. The maximum value of the refractive index is 2.79 at 5.72 eV for $CoCr_2O_4$, 6.81 at 0.01 eV for $CoMn_2O_4$ and 1.45 at 2.69 eV for $CoFe_2O_4$. We can therefore conclude that the maximum value of the refractive index is attributed to $CoMn_2O_4$. The maximum value of the observed extinction coefficient $k(\omega)$ corresponds to the 6.38 eV (4.34 eV) energy which belongs to the ultraviolet region, due to interband transitions of the majority (minority) states of $CoCr_2O_4$ ($CoFe_2O_4$) and at the energy of 0.01 eV the extinction coefficient $k(\omega)$ reaches its maximum value. The latter belongs to the infrared region, due to the interband transitions of the majority (minority) states of $CoCr_2O_4$ ($CoFe_2O_4$) and the majority states of $CoMn_2O_4$. This value corresponds to the zero of the dispersive parts $\varepsilon_1(\omega)$.

The reflectivity $R(\omega)$ started at 6.75%, 11.83% and 6.96% for minority spin channel and at 7.50%, 4.56% and 47.55% for the majority states, which leads to a total reflectivity of 14.50%, 16.41% and 55.75% in the infrared region for $CoCr_2O_4$, $CoFe_2O_4$ and $CoMn_2O_4$ respectively. Figure 5(e) shows for low energies, the reflectivity increases; then it decreases; then it increases again to reach a main peak at an energy of 25.10, 4.25 and 2.27 eV for $CoCr_2O_4$, $CoFe_2O_4$ and $CoMn_2O_4$ respectively. We have noticed that the spinel $CoMn_2O_4$ has the highest reflectivity followed by $CoCr_2O_4$ and $CoFe_2O_4$.

The total absorption coefficient $I(\omega)$ as a function of energy of the studied spinels is presented in Figure 5(f). In low energies, $I(\omega)$ increases considerably to reach its maximum value near ultraviolet region then it decreases. The strong peak is obtained at 22.38, 19.44 and 16.88 eV for $CoCr_2O_4$, $CoFe_2O_4$ and $CoMn_2O_4$ respectively. The $CoCr_2O_4$ has the highest absorption coefficient then $CoMn_2O_4$ and $CoFe_2O_4$. So we can consider that this spinels materials can be used as optoelectronic devices because they have a wide absorption band with a high absorption intensity.

The relationship between the oscillating electric field $E(\omega)$ and the current density $j(\omega)$ is presented by the optical conductivity $\sigma(\omega)$ (see ref [47]). And when $\omega \to 0$, it converts to electrical conductivity. The real part is directly related to the imaginary part from the following equation: $\sigma(\omega) = \frac{\omega}{4\pi}\varepsilon_2$. Figure 5(g) represents the spectrum of optical conductivity. From this spectrum we observe several peaks which corresponds to transitions interband transitions. Sharp edges occur at 2-16 eV (*ultraviolet region*). The optical conductivity of $CoMn_2O_4$ is larger than the $CoCr_2O_4$ and then $CoFe_2O_4$.

Finally, the energy loss function can be calculated from the dielectric function. It can be described by the expression cited in our previous work [48,49]. In regards to CoX_2O_4 ($X = Cr$, Mn and Fe) spinels (Figure 5(f)), There is a large energy loss in the energy range between 23-26 eV. The highest peak is around 25 eV. $CoCr_2O_4$ is the compound with the greatest energy loss then comes $CoCr_2O_4$ and finally the $CoFe_2O_4$.

4. Conclusions

Using methods based on the first-order density functional theory, systematic investigations were carried out to describe the structural and magnetic properties of CoX_2O_4 ($X = Cr$, Mn and Fe) spinel compounds while modifying the X cation. Obtaining the correct structures of the ground state is only possible if the electron–electron interactions between magnetic cations are introduced. All three compounds have a ferrimagnetic configuration. We noticed that at octahedral sites there is strong local structural distortion and for the $CoMn_2O_4$ compound global tetragonal distortions occurred. It was found that the chemical bonds between X cations and oxygen atoms decreased when iron atoms were replaced with chromium and then manganese atoms. Concerning the angles between the cobalt atoms and the oxygen atoms, they increase when changing from $CoFe_2O_4$ to $CoCr_2O_4$ to $CoMn_2O_4$. When the X cations are modified, the electronic properties of our spinels are significantly different, such as the band gap. The band structure of CoX_2O_4 ($X = Cr$, Mn and Fe) shows a direct band gap. When the atomic size of element X decreases the value of the band gap increases. Attempts are being made to understand trends in magnetic properties by correctly quantifying the associated quantities and trying to explain the relationship between electronic structures and local structural parameters. The lower part of the conduction band is dispersive, while the upper part of the valence band is less dispersive. Therefore, the mobility of holes in the valence band must be lower than that of electrons in the conduction band. The prediction of optical properties for an energy range from 0 to 30 eV is possible. The spectra of the absorption optic $\varepsilon_2(\omega)$ of all three compounds move towards a lower energy from $CoCr_2O_4$ to $CoMn_2O_4$ to $CoFe_2O_4$. We have noticed that $\varepsilon_1(0)$ decreases with increasing band gap, this fits well with Penn's model. We have noticed a large anisotropy in the real part $\varepsilon_1(\omega)$ of dielectric function for the $CoMn_2O_4$ compounds. The value of $n(0)$ increases when replacing the chromium atom with magnesium and subsequently the iron atom, following a trend opposite to that of the band gap. We have noticed that the spinel $CoMn_2O_4$ has the highest reflectivity followed by $CoCr_2O_4$ and $CoFe_2O_4$. The $CoCr_2O_4$ has the highest absorption coefficient then $CoMn_2O_4$ and $CoFe_2O_4$. The optical conductivity of $CoMn_2O_4$ is larger than the $CoCr_2O_4$ and then $CoFe_2O_4$. $CoCr_2O_4$ is the compound with the greatest energy loss then comes $CoCr_2O_4$ and finally the $CoFe_2O_4$. Which confirms the interest of these spinels for optical and optoelectronic device applications.

Acknowledgements

The authors (T. Ghellab, Z. Charifi, and H. Baaziz) would like to thank the general directorate for scientific research and technological development for their financial support during the realisation of this work

Disclosure statement

No potential conflict of interest was reported by the author(s).

References

[1] S. Jin, T.H. Tiefel, M. McCormack, R.A. Fastnacht, R. Ramesh and L.H. Chen, *Thousand fold change in resistivity in magnetoresistive La-Ca-Mn-O films*. Science. 264 (1994), pp. 413.

[2] H. Ohno, *Making nonmagnetic semiconductors ferromagnetic*. Science. 281 (1998), pp. 951.

[3] N.V. Kuleshov, V.P. Mikhialov and V.G. Scherbitsky, *Co-doped spinels: promising materials for solid state lasers*. Proc. SPIE. 175 (1994), pp. 2138.

[4] A. Jouini, A. Yoshikawa, A. Guyot, A. Breiner, T. Fukuda and G. Boulon, *Systematic analysis of structural and magnetic properties of spinel CoB_2O_4 (B=Cr, Mn and Fe) compounds from their electronic structures*. Opt. Mater. 30 (2007), pp. 47.

[5] K.G. Tshabalala, S.H. Cho, J.K. Park, S.S. Pitale, I.M. Nagpure, R.E. Kroon, H.C. Swart and O.M. Ntwaeaborwa, *Luminescent properties and X-ray photoelectron spectroscopy study of ZnAl2O4:Ce3+, Tb3+ phosphor*. J. Alloys Compds. 509 (2011), pp. 10115.

[6] Y.X. Li, P.J. Niu, L. Hu, X.W. Xu and C.C. Tang, *Monochromatic blue-green and red emission of rare-earth ions in $MgGa_2O_4$ spinel*. J. Lumin. 129 (2009), pp. 1204.

[7] P.J. Deren, K. Maleszka-Baginska, P. Gluchowski and M.A. Malecka, *Spectroscopic properties of Nd3+ in $MgAl_2O_4$ spinel nanocrystals*. J. Alloys Compds. 525 (2012), pp. 39.

[8] N. Menayuk, K. Dwight and A. Wold, *Ferrimagnetic spiral configurations in cobalt chromite*. J. Phys. France 25 (1964), pp. 528.

[9] K. Tomiyasu, J. Fukunaga and H. Suzuki, *Magnetic short-range order and reentrant-spin-glass-like behavior in $CoCr_2O_4$ and $MnCr_2O_4$ by means of neutron scattering and magnetization measurements*. Phys. Rev. B 70 (2004), pp. 214434.

[10] Y. Yamasaki, S. Miyasaka, Y. Kaneko, J.-P. He, T. Arima and Y. Torakuma, *Magnetic reversal of the ferroelectric polarization in a multiferroic spinel oxide*. Phys. Rev. Lett. 96 (2006), pp. 207204.

[11] D.H. Lyons, T.A. Kaplan, K. Dwight and N. Menyuk, *Classical theory of the ground spin-state in cubic spinels*. Phys. Rev. 126 (1962), pp. 540.

[12] L.J. Chang, D.J. Huang, W.-H. Li, S.-W. Cheong, W. Ratcli and J.W. Lyn, *Crossover from incommensurate to commensurate magnetic orderings in $CoCr_2O_4$*. J. Phys. Condens. Matt. 21 (2009), pp. 456008.

[13] T.H. Arima, Y. Yamasaki, T. Goto, S. Iguchi, K. Ohgushi, S. Miyasaka and Y. Tokura, *Spin–lattice coupling in ferroelectric spiral magnets: comparison between the cases of (Tb,Dy)MnO_3 and $CoCr_2O_4$*. J. Phys. Soc. Jpn. 76 (2007), pp. 023602.

[14] C. Ederer and M. Komelj, *Magnetic coupling in $CoCr_2O_4$ and $MnCr_2O_4$: an LSDA+U*. Phys. Rev. B. 76 (2007), pp. 064409.

[15] H. Zhang, W. Wang, E. Liu, X. Tang, G. Li, H. Zhang and G. Wu, *Compensation effect and magnetostriction in $CoCr_2$−$xFexO_4$*. Phys. Status Solidi B. 250 (2013), pp. 1287.

[16] R. Padam, S. Pandya, S. Ravi, A.K. Nigam, S. Ramakrishnan, A.K. Grover and D. Pal, *Magnetic compensation effect and phase reversal of exchange bias field across compensation temperature in multiferroic Co $(Cr0.95Fe0.05)_2O_4$*. Appl. Phys. Lett. 102 (2013), pp. 112412.

[17] R. Padam, S. Pandya, S. Ravi, A.K. Nigam, S. Ramakrishnan, A.K. Grover and D. Pal, *Magnetic compensation effect and phase reversal of exchange bias field across*

compensation temperature in multiferroic $Co(Cr0.95Fe0.05)_2O_4$. AIP Conf. Proc. 1512 (2013), pp. 1112.
[18] R. Padam. *PhD Thesis*, IIT Guwahati, 2014.
[19] H.G. Zhang, Z. Wang, E.K. Liu, W.H. Wang, M. Yue and G.H. Wu, *Site preference and compensation behavior in $Co(Cr, Mn)_2O_4$ system*. J. Appl. Phys. 117 (2015), pp. 17B735.
[20] C. Ederer and M. Komelj, *Magnetic coupling in $CoCr_2O_4$ and $MnCr_2O_4$: an LSDA+U study*. Phys. Rev. B 76 (2006), pp. 064409.
[21] D. Das and S.J. Ghosh, *Density functional theory based comparative study of electronic structures and magnetic properties of spinel ACr_2O_4 (A=Mn, Fe, Co, Ni) compounds*. J. Phys. D: Appl. Phys. 48 (2015), pp. 425001.
[22] K. Bouferrache, Z. Charifi, H. Baaziz, G. Uğur, Ş Uğur, B. Boyacıoğlu and H. Ünver, *Cation distribution effect on electronic, magnetic structure and optic properties in cobalt ferrites (Co1−yFey)Tet(CoyFe$_2$−y)OctO_4 with disordered spinel structure*. Phys. Scr. 95 (2020), pp. 105801.
[23] Y.H. Hou, Y.J. Zhao, Z.W. Liu, H.Y. Yu, X.C. Zhong, W.Q. Qiu, D.C. Zeng and L.S. Wen, *Structural, electronic and magnetic properties of partially inverse spinel $CoFe_2O_4$: a first-principles study*. J. Phys. D Appl. Phys. 43 (2010), pp. 445003.
[24] S. Ganguly, R. Chimata and B. Sanyal, *Overcoming magnetic frustration and promoting half-metallicity in spinel $CoCr_2O_4$ by doping with Fe*. Phys. Rev. B. 92 (2015), pp. 224417.
[25] M. Ye, S. Zhuravlev, S. Jaswal and E.Y. Tsymbal, *Ferroelectric switch for spin injection*. Appl. Phys. Lett. 87 (2005), pp. 222114.
[26] M. Gajek, M. Bibes, S. Fusil, K. Bouzehouane, J. Fontcuberta, A. Barthelemy and A. Fert, *Tunnel junctions with multiferroic barriers*. *Nat. Mater*. 6 (2007), pp. 296–302.
[27] P. Blaha, K. Schwarz, G.H.K. Madsen, D. Kvasnicka, J. Luitz and K. Schwarz. *Techn*. Universitat Wien, Wien, 2008.
[28] J.P. Perdew, K. Burke and M. Ernzerhof, *Generalized gradient approximation made simple*. Phys. Rev. Lett. 77 (1996), pp. 3865.
[29] L.M. Roth, *New method for linearizing many-body equations of motion in statistical mechanics*. Phys. Rev. Lett. 20 (1968), pp. 1431.
[30] J. van den Brink, M.B.J. Meinders and G.A. Sawatzky, *Influence of screening effects and inter-site Coulomb repulsion on the insulating correlation gap*. Physica B 682 (1995), pp. 206–207.
[31] G.K.H. Madsen and P. Novak, *Charge order in magnetite. An LDA+U study*. Euro. Phys Lett. 69 (2005), pp. 777.
[32] C. Herring. Magnetism, Vol. IV, G. T. Rado and H. Suhl, eds., Academic Press, New York, 1966, pp. 256–257.
[33] V.I. Anisimov, J. Zaanen and O.K. Andersen, *Band theory and Mott insulators: Hubbard U instead of stoner*. Phys. Rev. B. 44 (1991), pp. 943.
[34] O. Gunnarsson, O.K. Andersen, O. Jepsen and J. Zaanen, *Density-functional calculation of the parameters in the Anderson model: application to Mn in CdTe*. Phys. Rev. B. 39 (1989), pp. 1708.
[35] J.C. Slater, *Quantum theory of molecules and solids*, McGraw-Hill, New York, 1974.
[36] F.J. Teillet, F. Bouree and R.J. Krishnan, *Magnetic structure of $CoFe_2O_4$*. Magn. Magn. Mater. 123 (1993), pp. 93–96.
[37] B. Boucher, R. Buhl and M. Perrin, *Magnetic structure of cobalt manganite by neutron diffraction*. J. Appl. Phys. 39 (1968), pp. 632.
[38] N. Menyuk, K. Dwight and A. Wold, *Ferrimagnetic spiral configurations in cobalt chromite*. J. Phys. 25 (1964), pp. 528.

[39] S.J. Kim, S.W. Lee and C.S. Kim Japan, *Mössbauer studies on exchange interactions in $CoFe_2O_4$*. J. Appl. Phys. 40 (2001), pp. 4897.
[40] D. Das, R. Biswas and S. Ghosh, *Systematic analysis of structural and magnetic properties of spinel CoB_2O_4 (B=Cr, Mn and Fe) compounds from their electronic structures*. J. Phys. Condens. Matter. 28 (2016), pp. 446001.
[41] D.G. Wickham and W.J. Croft, *Crystallographic and magnetic properties of several spinels containing trivalent ja-1044 manganese*. J. Phys. Chem. Solids. 7 (1958), pp. 351.
[42] F.D. Murnaghan, *The compressibility of media under extreme pressures*. *Proc. Natl. Acad. Sci.* U. S. A 30 (1944), pp. 244.
[43] G. Hu, J.H. Choi, C.B. Eom, V.G. Harris and Y. Suzuki, *Structural tuning of the magnetic behavior in spinel-structure ferrite thin films*. Phys. Rev. B. 62 (2000), pp. R779.
[44] J.D. Dunitz and L.E. Orgel, *Electronic properties of transition-metal oxides – I: distortions from cubic symmetry*. J. Phys. Chem. Solids. 3 (1957), pp. 20.
[45] I.B. Berusker. *New York: Wiley*, 1996.
[46] D.G. Wickham and J.B. Goodenough, *Suggestion concerning magnetic interactions in spinels*. Phys. Rev. 115 (1959), pp. 115–1156.
[47] T. Ghellab, H. Baaziz, Z. Charifi, K. Bouferrache, M.A. Saeed and A. Telfah, *Ab initio full-potential study of the fundamental properties of chalcopyrite semiconductors XPN2 (X=H, Cu)*. Mater. Res. Express. 6 (2019), pp. 075906.
[48] T. Ghellab, Z. Charifi, H. Baaziz, Ş Uğur, G. Uğur and F. Soyalp, *First principles study of hydrogen storage material NaBH4 and LiAlH4 compounds: electronic structure and optical properties*. Phys. Scr. 91 (2016), pp. 045804.
[49] T. Ghellab, Z. Charifi, H. Baaziz, K. Bouferrache and B. Hamad, *Electronic structure and optical properties of complex hydrides LiBH4 and NaAlH4 compounds*. Int. J. Energy Res. (2019), pp. 1–15.